Article

Cell Metabolism

MYC/PGC-1α Balance Determines the Metabolic Phenotype and Plasticity of Pancreatic Cancer Stem Cells

Graphical Abstract

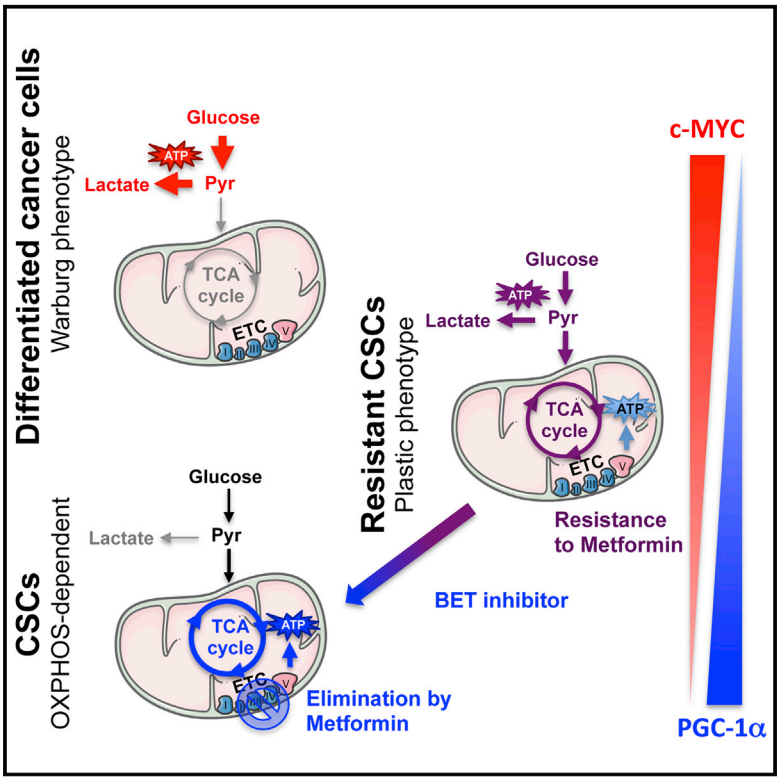

Highlights

- Pancreatic CSCs rely on mitochondrial OXPHOS and show reduced metabolic plasticity
- Mitochondrial inhibition effectively eliminates pancreatic CSC
- MYC/PGC-1α balance controls the metabolic phenotype of PDAC cells
- MYC targeting prevents resistance/restores the response to metformin in resistant CSCs

Authors

Patricia Sancho,
Emma Burgos-Ramos,
Alejandra Tavera, ..., Mariia Yuneva,
Bruno Sainz, Jr.,
Christopher Heeschen

Correspondence

p.sancho@qmul.ac.uk (P.S.),
c.heeschen@qmul.ac.uk (C.H.)

In Brief

Sancho et al. show that pancreatic cancer stem cells (CSCs) are especially vulnerable to mitochondrial-targeted therapies (i.e., metformin) due to their strong reliance on oxidative metabolism. The MYC/PGC-1α balance acts as the main determinant for this OXPHOS dependency, and genetic/pharmacological targeting of MYC restores metformin response in resistant CSCs.

Sancho et al., 2015, Cell Metabolism *22*, 590–605
October 6, 2015
http://dx.doi.org/10.1016/j.cmet.2015.08.015

CellPress

Cell Metabolism
Article

MYC/PGC-1α Balance Determines the Metabolic Phenotype and Plasticity of Pancreatic Cancer Stem Cells

Patricia Sancho,[1,2,*] Emma Burgos-Ramos,[2] Alejandra Tavera,[2] Tony Bou Kheir,[1] Petra Jagust,[1] Matthieu Schoenhals,[1] David Barneda,[1] Katherine Sellers,[5] Ramon Campos-Olivas,[3] Osvaldo Graña,[4] Catarina R. Viera,[2] Mariia Yuneva,[5] Bruno Sainz, Jr.,[2] and Christopher Heeschen[1,2,*]

[1]Centre for Stem Cells in Cancer & Ageing, Barts Cancer Institute, Queen Mary University of London, London EC1M 6BQ, UK
[2]Stem Cells & Cancer Group, Molecular Pathology Programme
[3]Spectroscopy and NMR Unit
[4]Bioinformatics Unit and Structural Biology and Biocomputing Programme
Spanish National Cancer Research Centre (CNIO), Madrid 28029, Spain
[5]The Francis Crick Institute, Mill Hill Laboratories, The Ridgeway, London NW7 1AA, UK
*Correspondence: p.sancho@qmul.ac.uk (P.S.), c.heeschen@qmul.ac.uk (C.H.)
http://dx.doi.org/10.1016/j.cmet.2015.08.015

SUMMARY

The anti-diabetic drug metformin targets pancreatic cancer stem cells (CSCs), but not their differentiated progenies (non-CSCs), which may be related to distinct metabolic phenotypes. Here we conclusively demonstrate that while non-CSCs were highly glycolytic, CSCs were dependent on oxidative metabolism (OXPHOS) with very limited metabolic plasticity. Thus, mitochondrial inhibition, e.g., by metformin, translated into energy crisis and apoptosis. However, resistant CSC clones eventually emerged during treatment with metformin due to their intermediate glycolytic/respiratory phenotype. Mechanistically, suppression of MYC and subsequent increase of PGC-1α were identified as key determinants for the OXPHOS dependency of CSCs, which was abolished in resistant CSC clones. Intriguingly, no resistance was observed for the mitochondrial ROS inducer menadione and resistance could also be prevented/reversed for metformin by genetic/pharmacological inhibition of MYC. Thus, the specific metabolic features of pancreatic CSCs are amendable to therapeutic intervention and could provide the basis for developing more effective therapies to combat this lethal cancer.

INTRODUCTION

Patients with pancreatic ductal adenocarcinoma (PDAC) suffer from very poor outcome, and the incidence is still rising, presumably related to the increased prevalence of diabetes and metabolic syndrome as major risk factors, which could make it the second most frequent cause of cancer death by 2030 (Rahib et al., 2014). The vast majority of patients is diagnosed at advanced stage and dies within 12 months due to lack of effective treatments (Siegel et al., 2012). During this time, many patients also suffer from rapidly declining performance as well as cachexia so that palliative care becomes the prevailing approach for these patients (Hidalgo, 2010). Consequently, PDAC represents a major unmet medical need with strong socioeconomic and humanitarian implications.

At least one possible explanation for the poor outcome of PDAC is that only scant attention has been paid to targeting cancer stem cells (CSCs) as a small, but highly tumorigenic and metastatic subpopulation of cancer cells. Indeed, convincing evidence now demonstrates that cancer heterogeneity not only is generated by genetically distinct subclones, but is also driven by phenotypic and functional heterogeneity within each subclone, resulting in a hierarchical organization of the tumor (Hermann et al., 2007; Li et al., 2007; Lonardo et al., 2011). At the apex of this hierarchy are populations of CSCs capable of self-renewal, bearing long-term in vivo tumorigenicity as well as generating more differentiated progenies constituting epigenetically defined intraclonal bulk (Miranda-Lorenzo et al., 2014). Even more importantly, these cells determine the metastatic behavior of PDAC and represent an important source for disease relapse (Hermann et al., 2007). Thus, targeting CSCs should represent an integral component for developing more effective treatment strategies (Gallmeier et al., 2011; Lonardo et al., 2011; Mueller et al., 2009).

We have recently demonstrated that these heterogeneous populations of pancreatic cancer cells differ in their response to metformin (Lonardo et al., 2013). While for the bulk of more differentiated cancer cells (non-CSCs) metformin induced cell-cycle arrest, CSCs actually underwent rapid apoptotic death. Subsequent in vivo studies in established patient-derived xenografts (PDX) showed that metformin stalled tumor progression or even induced disease regression. These data suggested a distinct metabolic phenotype for CSCs and, indeed, here we demonstrate that pancreatic CSCs strongly depend on the mitochondrial oxidative phosphorylation (OXPHOS), whereas non-CSCs mostly rely on glycolysis. Interestingly, CSCs showed reduced metabolic plasticity based on their limited ability to switch to glycolysis upon mitochondrial inhibition. This was related to reduced levels of c-MYC expression and inversely increased levels of PGC-1α in CSCs versus non-CSCs. However, eventually tumors relapsed under metformin due to emergence of resistant CSCs with an intermediate metabolic

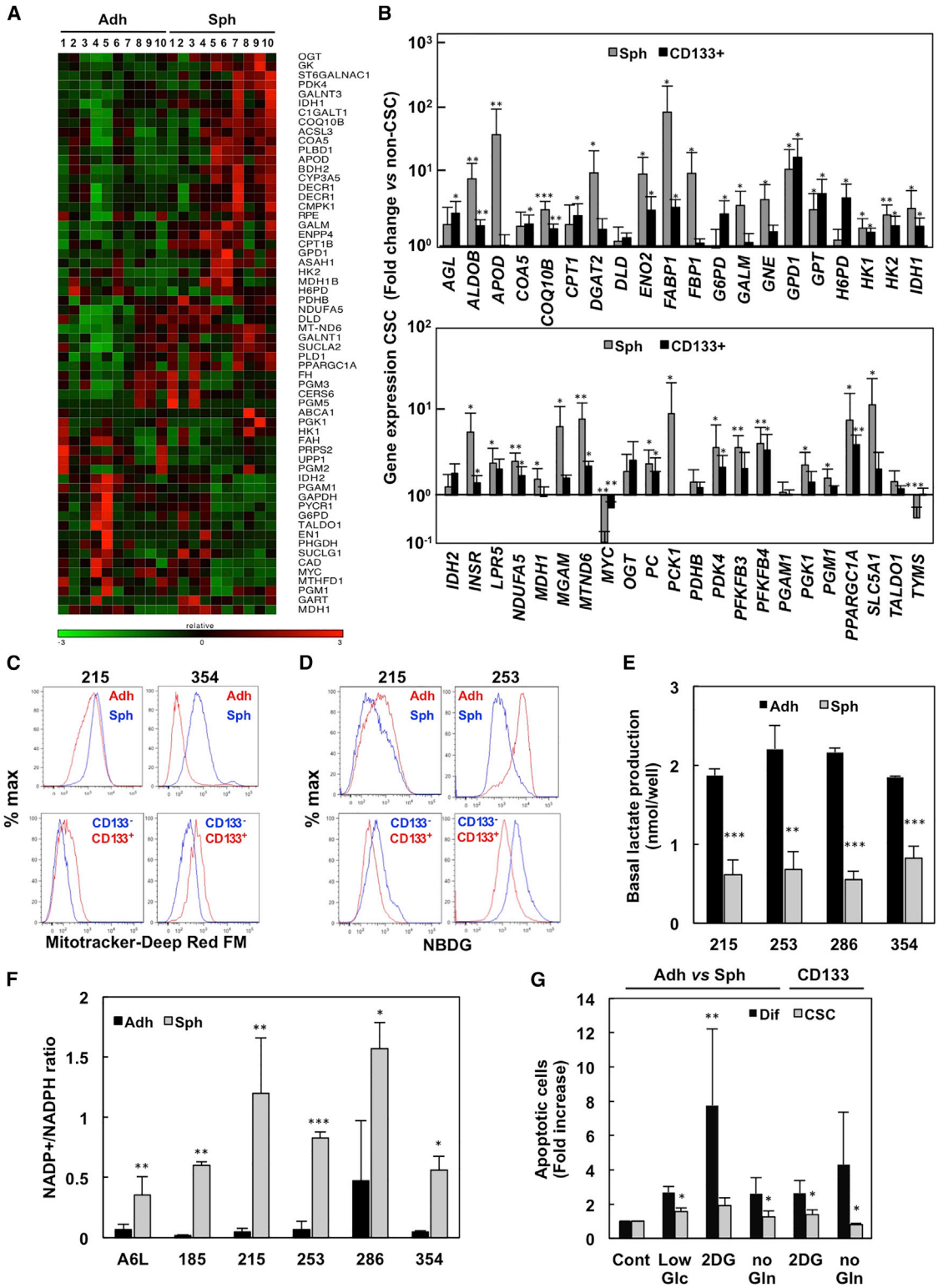

Figure 1. Pancreatic CSCs Display Distinct Metabolic Features

(A) Heatmap of 60 metabolism-related genes identified by RNA-seq using five primary PDAC cultures (PDX-185, 215, 253, 265, and 354) grown as either adherent (Adh) or anchorage-independent cultures (spheres, Sph) analyzed in biological duplicates.

(B) Representative samples from the RNA-seq experiment (PDX-215, 253, 354) as well as CD133−/+ sorted cells from the same PDXs were validated by real-time PCR.

(C) Mitochondrial mass as determined by flow cytometry using MitoTracker Deep Red-FM. Representative plots.

(legend continued on next page)

phenotype with increased c-MYC expression. Intriguingly, genetic or pharmacological targeting of c-MYC inhibited/reversed this phenotype, suggesting a multimodal strategy for most efficient metabolic targeting of pancreatic CSCs.

RESULTS

Pancreatic CSCs Display Metabolic Features Compatible with Oxidative Metabolism

To define the metabolic features of cells enriched for CSC, we used anchorage-independent sphere cultures (spheres) versus mostly differentiated cells in adherent cultures (adherent cells) Figure S1A); we first performed RNA-seq analyses for primary cultures derived from five different PDX models (Jimeno et al., 2009; Lonardo et al., 2011). A heatmap selecting a total of 60 metabolism-related genes differentially expressed in spheres versus adherent cells suggested distinct metabolic phenotypes (Figures 1A and S1B). Besides upregulation of genes related to glycosylation and lipid metabolism, spheres also displayed enhanced expression for several TCA enzymes and mitochondrial OXPHOS components. In contrast, adherent cells showed upregulation of genes related to glycolysis, pentose phosphate pathway (PPP), and amino acid synthesis. Data were confirmed by qRT-PCR or PCR array designed for carbohydrate metabolism using spheres and $CD133^+$ cells in order to further enrich for CSC, respectively (Figure 1B).

Consistently, spheres or $CD133^+$ cells showed increased mitochondrial mass, but reduced glucose uptake, lactate production (both in normoxic or hypoxic conditions), and mitochondrial ROS levels (Figures 1C–1E, S1C, and S1D). In addition, their NADP/NADPH ratio was increased compared to adherent or $CD133^-$ cells (Figure 1F), in line with the observed lower expression of PPP enzymes. Spheres were also less sensitive to metabolic challenges such as glucose or glutamine deprivation or inhibition of glycolysis (Figures 1G and S1E).

Next, we performed ^{13}C-glucose (U-^{13}C-Glc) flux analyses using nuclear magnetic resonance (NMR) spectroscopy for supernatants or gas chromatography-mass spectrometry (GC-MS) for cell extracts. Notably, for all experiments, both spheres and adherent cells were preincubated in serum-free conditions, resulting in similar proliferation levels (Figure S2A) and cellular viability (data not shown). Glucose flux analysis demonstrated reduced glucose uptake and ^{13}C-lactate release in spheres (Figure S2B) indicative of diminished glycolytic flux. These changes detected in the supernatant were corroborated by measurements in respective cellular extracts, showing in spheres a lower flux of ^{13}C-Glc towards lactate (Figure S2C). Interestingly, ^{13}C labeling of Ribose-5-P was also reduced in spheres, confirming a diminished activity of the PPP in CSC-enriched conditions (Figure S2D). In contrast, the glucose-derived ^{13}C label was significantly enriched in the Krebs cycle intermediates succinate, fumarate, malate, and citrate (Figures S2E–S2H). Thus, CSC-enriched cultures bear a distinct metabolic profile with higher catabolism of glucose through the Krebs cycle, while adherent cells consume more glucose and subsequently show higher flux towards lactate and PPP, consistent with a "Warburg effect-like" profile.

CSCs Bear Enhanced Mitochondrial Respiration and Impaired Metabolic Plasticity

To functionally validate these findings that suggest an enhanced mitochondrial activity of CSCs versus non-CSCs, we measured their oxygen consumption rates (OCR) in the presence or absence of distinct inhibitors of mitochondrial function (Figures 2A and S3A). Baseline OCR was significantly increased in sphere-derived or $CD133^+$ cells isolated from five different tumors as compared to their differentiated counterparts (Figure S3B). Specifically, while the non-mitochondrial oxygen consumption was also significantly higher in CSC-enriching conditions, the differences for mitochondrial oxygen consumption were even more striking (Figures 2B, S3B, and S3C). To ensure strict validity of this key finding, we took several measures. First, we excluded any impact of culture conditions by reproducing the data in cells derived from the same primary culture and sorted for the CSC markers CD133 or autofluorescence, respectively (Figures 2B and S3B–S3D). Second, we validated the data in cells derived from freshly digested tumors ($CD133^-$ versus $CD133^+$), also excluding potential cell culture artifact. Third, we ruled out a potential influence of intratumoral heterogeneity by reproducing above data derived from the heterogeneous parental PDX-185 in a tumor that arose from a single CSC originally isolated from PDX-185. Even though basal OCR slightly differed between the polyclonal parental tumor and the monoclonal derivative tumor, suggestive of an interdependence of the respective genetic background and the respiratory phenotype, differences in baseline OCR between CSCs and non-CSCs remained significant, confirming the robustness of our findings.

Cancer cells regularly increase their glycolytic activity to maintain stable ATP levels when mitochondrial function is inhibited (Wu et al., 2007), which could also be reproduced for pancreatic non-CSCs and translated into increased lactate production as evidenced by a concomitant ECAR rise (Figure 2C). A similar response was observed upon Glc injection for starved non-CSCs (Figure 2D). In contrast, such increase in ECAR was severely blunted in CSCs (Figures 2C–2E and S3D, right panel). Importantly, findings were independent of culture conditions, origin of the cells (in vitro versus in vivo), and genetic background, even though differences were less prominent for the monoclonal single-cell-derived tumor (Figure 2E). This limited glycolytic capacity of CSCs eventually translated into a significant drop in ATP levels and subsequent energy crisis upon mitochondrial inhibition in spheres, whereas adherent cells showed only a minor response (Figure 2F). On the other hand, inhibition of glycolysis caused a marked drop in ATP levels in adherent cells, demonstrating strong dependence on the

(D) Glucose uptake by 2-NBDG incorporation by flow cytometry. Representative plots.
(E) Lactate production.
(F) NADP/NADPH ratio.
(G) Number of apoptotic cells after 72 hr of incubation in the indicated conditions. Glc, glucose; Gln, glutamine.
In (C), (D), and (G), CSCs represent CSC-enriched sphere cultures (Sph) or $CD133^+$ cells, while differentiated cultures are adherent cultures (Adh) or $CD133^-$ cells. Data in (B), (E), (F), and (G) are presented as mean ± SEM. See also Figure S1.

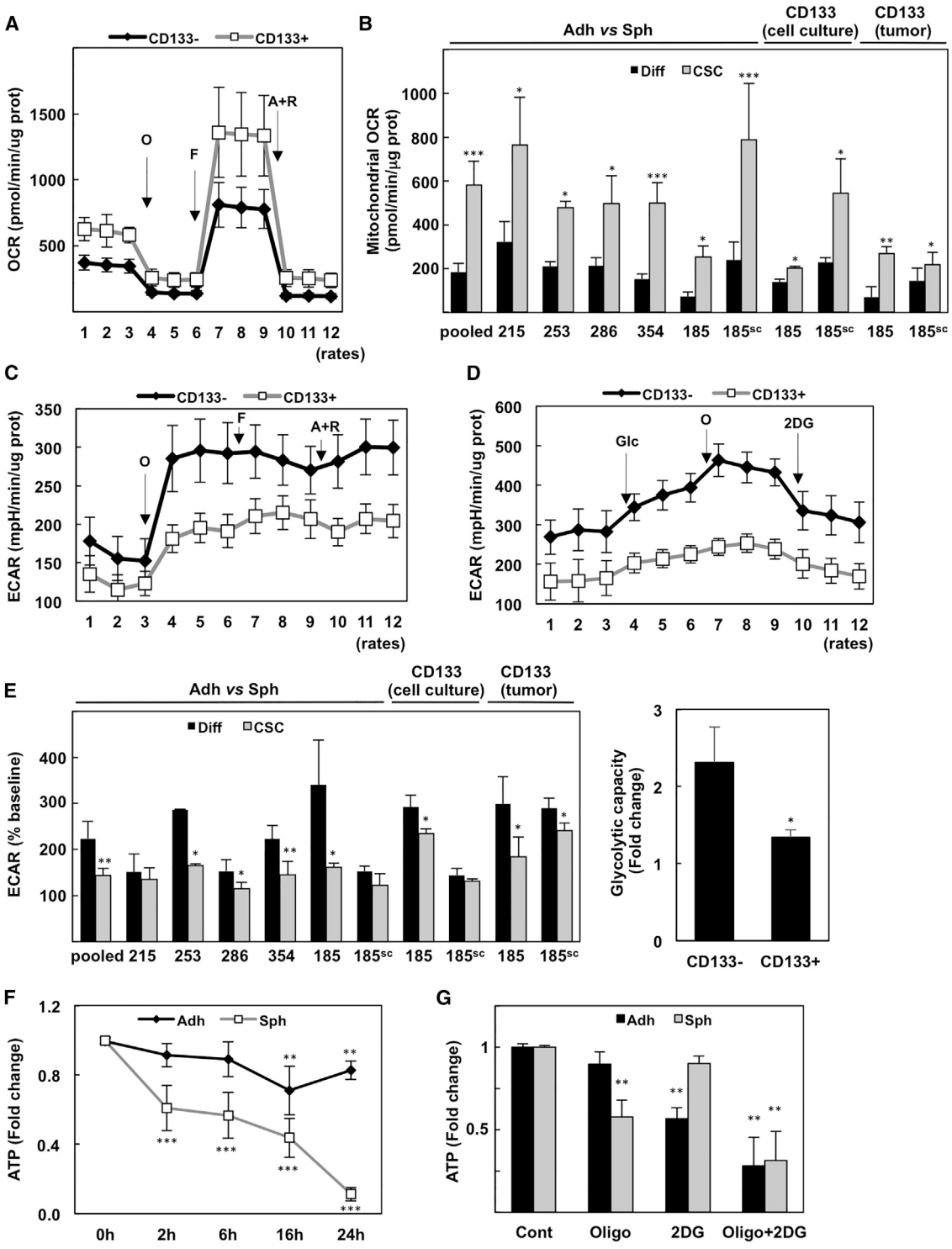

Figure 2. CSCs Bear Enhanced Mitochondrial Respiration and Impaired Glycolytic Plasticity

Oxygen consumption rate (OCR) and extracellular acidification rate (ECAR) were determined using the XF Extracellular Flux Analyzer comparing differentiated cells (Adh or CD133$^-$) and CSC-enriched cultures (Sph or CD133$^+$). When indicated, CD133$^-$ and CD133$^+$ cells were sorted from primary sphere cultures (CD133, cell culture) or freshly digested tumors (CD133, tumor) from either the parental 185 PDX (185) or a tumor obtained upon injection of a single CSC from a 185 primary culture (185^{sc}).

(A) Oxygen consumption rate (OCR). Pooled data for sorted cells from PDX-215, 253, and 354 primary cultures, which were subsequently treated by injection of oligomycin (O), FCCP (F), and antimycin plus rotenone (A+R) into the culture medium.

(B) Mitochondrial oxygen consumption (ATP-linked + proton leak).

(legend continued on next page)

Warburg effect, while the effect on spheres was minor (Figure 2G). Taken together, our data conclusively demonstrate that CSCs bear reduced metabolic plasticity, mostly relying on OXPHOS, and thus are not able to effectively induce glycolysis to compensate for reduced ATP production upon mitochondrial inhibition.

Mitochondrial Targeting Effectively Diminished CSCs

We have previously shown that metformin, which exerts considerable inhibition of mitochondrial complex I, induced apoptosis preferentially in CSC-enriched cultures while provoking cell-cycle arrest in adherent cells (Lonardo et al., 2013). To demonstrate a causal link to the reduced metabolic plasticity of CSCs, metformin was injected into the medium, resulting in a rapid and dose-dependent drop in OCR, which became more apparent in low Glc conditions (Figures 3A–3C). Indeed, metformin treatment rendered spheres unable to respond to FCCP, which suggests a disruption of the proton gradient consistent with complex I inhibition, similar to the one provoked by rotenone (Figure 3D). In addition, we found that long-term treatment with metformin moderately inhibited mitochondrial oxygen consumption in both CSC-enriched or -depleted conditions (Figure 3E), even though the effect was more pronounced in spheres ranging from 20%–60%. This was accompanied by an increment in lactate production and NADPH accumulation (Figures 3F and 3G), most likely as a result of the relative enrichment of the non-CSC fraction following preferential elimination of CSCs as evidenced by a decline in the content of $CD133^+$ cells (Figure 3H).

The fact that a rather moderate inhibition of mitochondrial oxygen consumption by metformin induces such a marked reduction in CSCs indicates a particular vulnerability of CSCs to inhibition of mitochondrial function and renders this approach a potentially attractive strategy to efficiently eliminate these highly tumorigenic cells. To further validate this concept, we studied other inhibitors of mitochondrial function: the specific complex I inhibitor rotenone, the mitochondrial ROS inducer menadione, and the ATP synthase inhibitor resveratrol (which may also affect other cellular targets), which were all capable of dose-dependently inhibiting OCR (Figure 4A). When titrated to achieve an equivalent level of OCR inhibition as induced by metformin, all compounds decreased ATP content to a level similar to that of the ATP synthase inhibitor oligomycin (Figure 4B) and subsequently induced AMPK activation in spheres (Figure 4C). Contrastingly, in adherent cells these treatments rather enhanced lactate production (Figure 4D) and, as a result, these cells did not suffer from a pronounced drop in ATP levels (data not shown), whereas the energy crisis in CSC-enriched cultures resulted in enhanced ROS production and eventually apoptosis (Figures 4E, S4A, and S4B). This effect translated into significantly decreased CSC activity in vitro and in vivo (Figures 4G–4I, S4C, and S4D).

However, despite these impressive initial treatment effects of metformin transforming highly aggressive in vivo PDX models into stable disease, tumors eventually progressed, irrespective of concomitant treatment with gemcitabine (Lonardo et al., 2013). As this represents a serious limitation for the proposed treatment strategy, we aimed to reproduce such acquisition of resistance in vitro for further mechanistic exploration. Indeed, primary cultures derived from various PDX models became resistant to metformin as well as resveratrol, although we did not observe the outgrowth of resistant clones upon treatment with menadione or rotenone over 60 days (Figure S4E). Consistently, long-term treatment of spheres with menadione or rotenone translated into a drastic decrease in $CD133^+$ cells as well as reduced sphere and colony formation, respectively (Figures S4F and S4G). Together, these results corroborate our finding that inhibition of mitochondrial activity induces energy crisis and apoptosis in pancreatic CSCs. Importantly, however, resistance seems to occur preferentially in metformin-treated cells and was not apparent for menadione, which combines inhibition of complex I and induction of ROS, rendering this approach a promising strategy to more thoroughly eliminate CSCs.

Metformin-Resistant CSCs Display an Intermediate Metabolic Phenotype

Next, we functionally compared untreated versus metformin-treated tumors, both while still responsive as well as during relapse (Figure 5A). First, we confirmed that tumors at different stages expressed at least one of the transporters mandatory for metformin uptake (*OCT1-3*) (Figure S5A). While metformin treatment irreversibly depleted cancer-associated fibroblasts, the cancer cell compartment, although greatly diminished during the sensitive phase, eventually relapsed in resistant tumors (Figures 5B, S5B, and S5C). Importantly, the CSC content, defined as $EPCAM^+$ cells co-expressing either CD44, CD133, or CXCR4, was reduced in sensitive tumors but had expanded again in resistant tumors (Figures 5B and S5C). Consistently, pluripotency-related genes were also decreased in sensitive tumors, but expression levels had relapsed in resistant tumors (Figure S5D). To elucidate whether resistance to metformin is occurring in all contained CSC subclones or predominantly occurring in certain subsets of CSCs, we tracked clonal distribution by implanting tumors stably expressing a barcode library. Interestingly, relapsed tumors showed a reduced clonal heterogeneity as evidenced by enrichment for certain barcodes, indicative of a positive selection and subsequent expansion of CSC subclones during metformin treatment (Figure 5C). Interestingly, however, CSCs contained in relapsing resistant tumors demonstrated reduced stemness properties as demonstrated by diminished sphere formation capacity (Figure S5E) and content of CSC marker positive cells (Figure S5F) as compared to sensitive tumors.

(C) ECAR simultaneously recorded to OCR as shown in (A).
(D) ECAR measurement in cells sorted for CD133 and subjected to sequential injections of glucose (Glc), oligomycin (O), and 2-deoxyglucose (2DG) into the medium.
(E) Glycolytic capacity, measured as the percentage of ECAR increase after mitochondrial inhibition (left) or glucose and oligomycin injection (right).
(F) ATP kinetic following injection of oligomycin.
(G) ATP content after 6 hr of treatment with the indicated compounds.
Data are represented as mean ± SEM. *$p < 0.05$, **$p < 0.01$, ***$p < 0.001$. See also Figure S3.

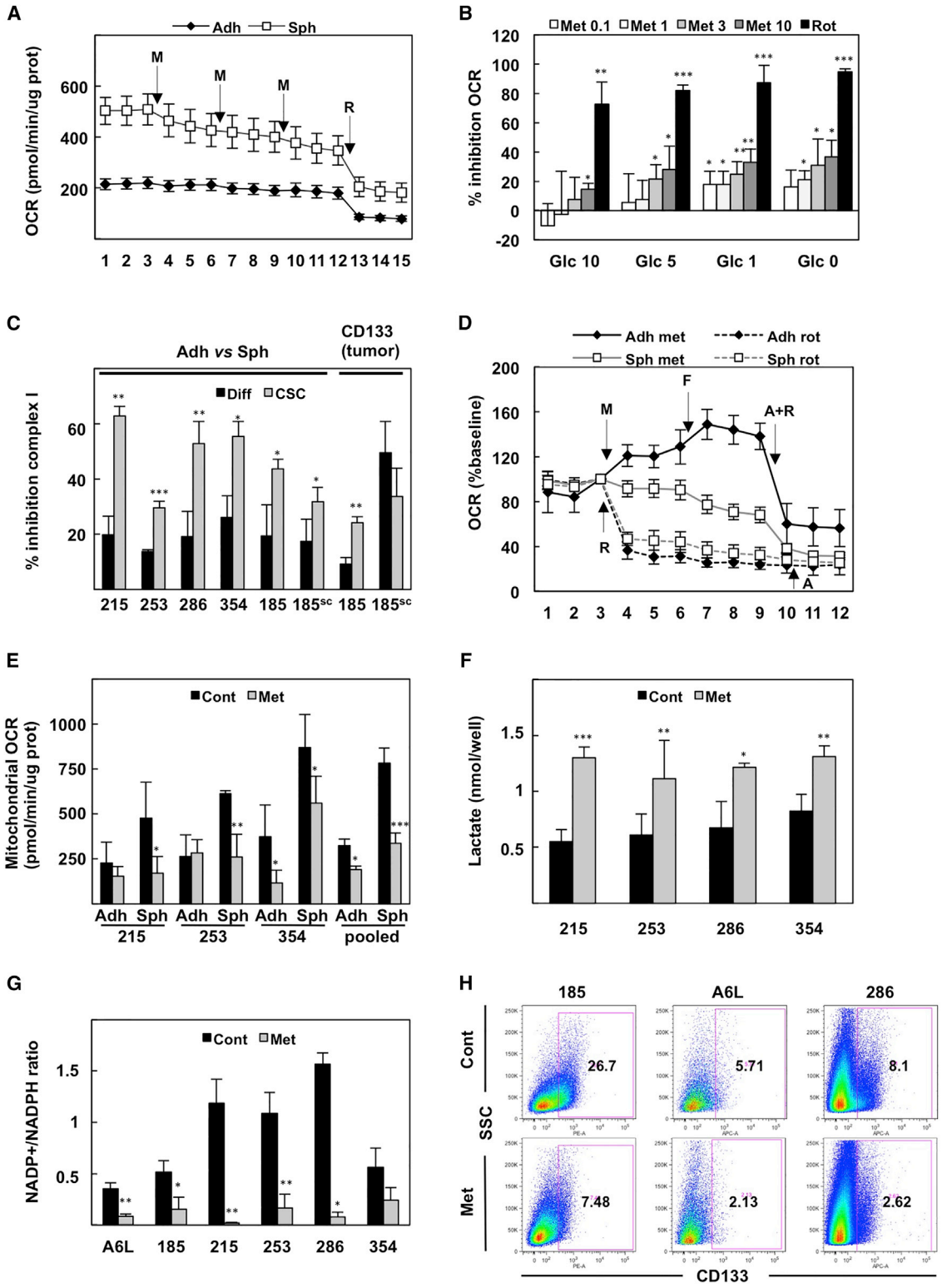

Figure 3. Metformin Inhibits Mitochondrial Respiration and Promotes Metabolic Reprogramming of CSCs

Adherent cultures or second-generation spheres were treated with 3 mM metformin (Met).

(A) OCR upon sequential metformin (M) injections. Rotenone (R) was used to completely block complex I activity.

(B) Percent OCR inhibition achieved by the indicated metformin doses or rotenone for decreasing glucose concentrations.

(C) Complex I activity inhibition by metformin, calculated as percentage of the inhibition obtained with rotenone, set as 100%.

(legend continued on next page)

Subsequent analysis of the metabolic features of CSCs (spheres or CD133$^+$ cells) expanding under metformin treatment indicated reduced basal and mitochondrial oxygen consumption compared to treatment-naive CSCs, while no significant changes could be found in respective differentiated counterpart populations (Figures 5D and 5E). Consistently, resistant CSC-enriched cultures showed increased glucose uptake (Figure S5G) and ^{13}C-lactate release upon incubation with ^{13}C-Glc (Figure S6A), suggesting enhanced basal glycolytic activity. Indeed, resistant CSCs displayed increased glycolytic capacity reaching levels comparable to that of differentiated cells (Figure 5F). Interestingly, further analysis by GC-MS indicated that resistant spheres not only showed higher flux of ^{13}C-Glc towards lactate as compared to sensitive spheres, but also enhanced flux into the PPP as evidenced by increased production of ^{13}C-Ribose-5-P (Figure S6B). However, no changes were found for ^{13}C enrichment in Krebs cycle intermediates (Figure S6C and data not shown), suggesting that resistant spheres flux glucose into the mitochondria as efficiently as sensitive ones. These data demonstrate that a subset of CSCs is equipped with enhanced glycolytic capacity, and therefore less susceptible to mitochondrial targeting, and eventually becomes the main driver of tumor propagation resulting in disease relapse. As such, while resistant cells were still able to respond to mitochondrial targeting and showed reduced complex I activity (Figure S5H), neither metformin nor resveratrol were capable of inducing apoptosis in these cells (Figure 5G), indicative of enhanced metabolic plasticity. Interestingly, as opposed to metformin, which bears long-term anti-oxidative properties (Batandier et al., 2006), the ROS inducer menadione still demonstrated significant toxicity, which may explain the apparent lack of resistance to menadione (Figure S4).

MYC/PGC-1α Ratio Determines the Metabolic Phenotype of CSCs

The outgrowth of CSC populations with an intermediate metabolic phenotype following metformin treatment enabled us to further elucidate the underlying molecular mechanism. First, we compared the carbohydrate metabolism-related expression profile of sensitive versus resistant CSC-enriched cultures derived from three different PDX models. Sensitive spheres exhibited increased expression of genes implicated in mitochondrial function and biogenesis (*COQ10B*, *NDUFA5*, *PPARGC1A*), while *MYC*, capable of regulating both glycolysis and mitochondrial activity, was significantly suppressed compared to adherent cells (Figures 6A and S6D). Expression levels in resistant spheres reached intermediate levels positioned between sensitive spheres and adherent cells, thus further corroborating our finding that resistant CSCs bear an intermediate metabolic phenotype. Moreover, withdrawal of metformin in resistant cells reversed the metabolic phenotype toward that of sensitive ones, with increased *PGC1A* levels and mitochondrial OCR (Figures S6E and S6F). These data suggest that, indeed, the main feature of resistant cells relies in their enhanced metabolic plasticity that is more receptive to changes in the environment.

To functionally validate the role of PGC-1α in determining the metabolic features of CSCs, we knocked down *PGC1A* in spheres using two different shRNA sequences cloned into an inducible expression system. *PGC1A* expression levels were reduced by at least 50% after 72 hr of doxycycline treatment, which was accompanied by a consistent decrease in mitochondrial respiration (Figure 6B). In line with above studies, CSC frequency as evidenced by sphere formation capacity was significantly reduced (Figure 6C). As the outgrowth of metformin-resistant CSCs suggested a certain degree of metabolic heterogeneity within the CSC compartment, we next isolated cells based on CD133 expression and their mitochondrial mass as a surrogate for *PGC1A* expression. As predicted, CD133$^+$/Mito^{high} cells showed highest CSC activity, followed by CD133$^+$/Mito^{low} cells, as demonstrated by increased expression of pluripotency-associated genes, in vitro self-renewal, and in vivo tumorigenicity (Figures 6D–6F). Interestingly, CD133$^+$/Mito^{high} cells displayed exclusive lethality in response to metformin treatment (Figure 6G), whereas CD133$^+$/Mito^{low} cells were resistant to metformin, although this came at the expense of reduced stemness.

MYC Inhibition Increases Mitochondrial Respiration, Restoring Response to Metformin and Full Stemness in Metformin-Resistant CSCs

Next, we investigated the role of *MYC* for the metabolic features of CSCs. Expression of *MYC* is tightly regulated by a complex network of positive and negative regulators, in which miRNAs play an important role (Jackstadt and Hermeking, 2015). Intriguingly, while *MYC* expression did not correlate with miR-429 (data not shown), *MYC* inversely correlated with the expression of miR-34 (Figure S7A), a miRNA that demonstrably plays an important role in pancreatic CSC self-renewal and cell-fate determination, respectively (Nalls et al., 2011). To further explore the contribution of *MYC* to the metabolic phenotype of pancreatic cancer (stem) cells, we modulated *MYC* expression by different means: (1) pharmacological inhibition by JQ-1, which resulted in a dose-dependent reduction of c-MYC expression (Figures 7A and 7B); (2) *MYC* knockdown using two different inducible shRNAs (Figure 7B, lower left panel); and (3) *MYC* overexpression (Figure 7B, lower right panel). Strikingly, *PGC1A* expression inversely correlated with *MYC* expression, implying that *MYC* may act as an upstream inhibitor of PGC-1α. As in silico prediction also suggested that the *PGC1A* promoter bears three putative MYC binding sites, we performed ChIP analysis, indicating that MYC is indeed directly binding to the *PGC1A* promoter (Figure S7B), and luciferase reporter assays confirmed its inhibitory activity on *PGC1A* expression (Figure S7C).

Consistently, *MYC* knockdown or pharmacological inhibition of MYC resulted in enhanced *PGC1A* expression and subsequently enhanced mitochondrial oxygen consumption, while

(D) OCR upon sequential injection of metformin (M), FCCP (F), and antimycin + rotenone (A+R) versus rotenone (R), FCCP (F), and antimycin (A).
(E) Mitochondrial oxygen consumption at 96 hr.
(F) Lactate production in spheres on day 7.
(G) NADP$^+$/NADPH ratio in spheres on day 7.
(H) CD133$^+$ cell content as assessed by flow cytometry on day 7.
Data in (A)–(G) are presented as mean ± SEM. *p < 0.05, **p < 0.01, ***p < 0.001.

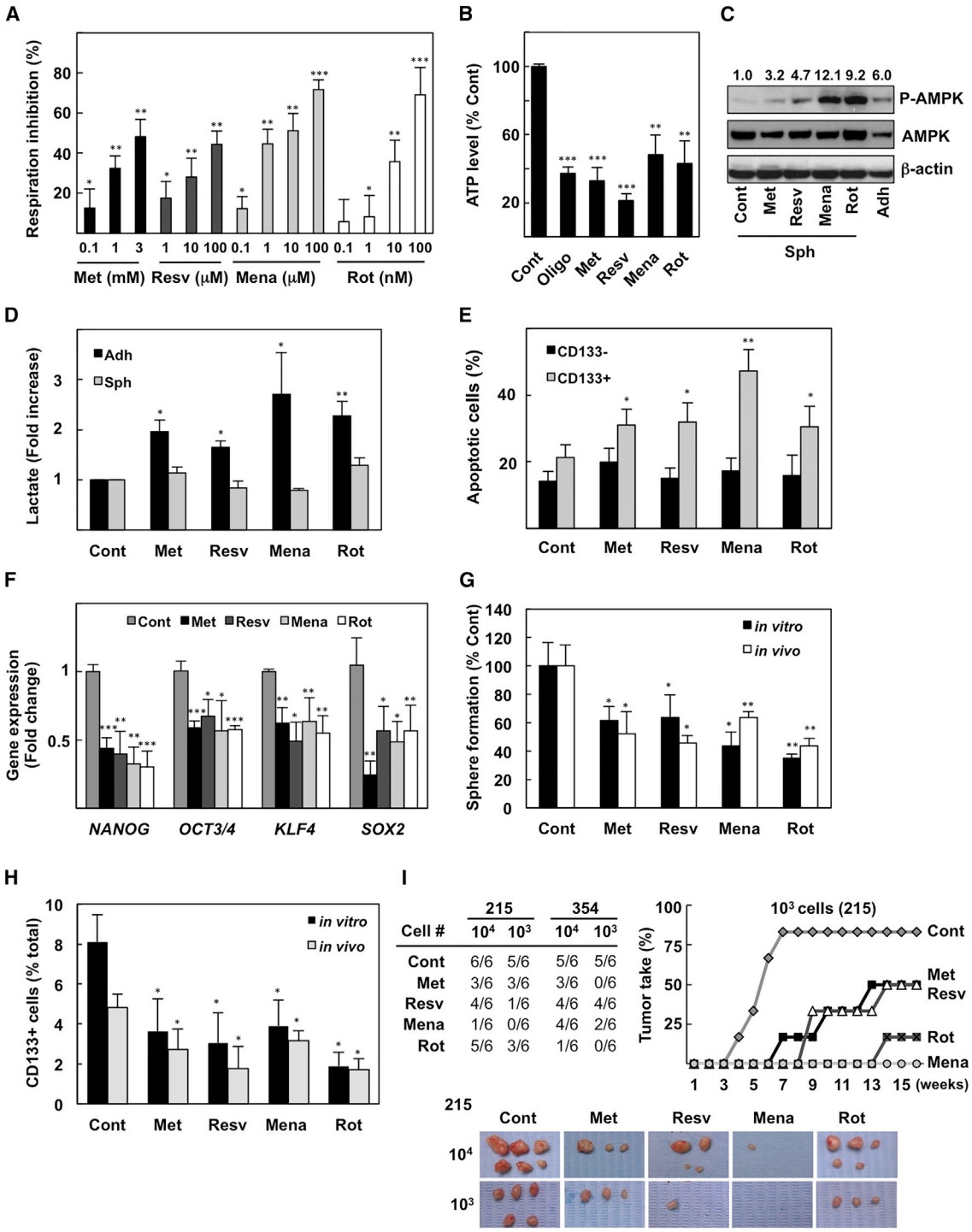

Figure 4. Diverse Panel of Mitochondrial Inhibitors Effectively Targets CSCs, Mimicking Metformin Effects

Except when indicated otherwise, adherent and second-generation sphere cultures were treated with 3 mM metformin (Met), 50 μM resveratrol (Resv), 10 μM menadione (Mena), or 10 nM rotenone (Rot).

(A) OCR inhibition in spheres after 16 hr of treatment.

(B) ATP in spheres after 6 hr. Oligomycin (Oligo; 1 μM) was included as positive control.

(C) AMPK activation at 16 hr. Representative western blots for PDX-354.

(D) Lactate production in spheres at 72 hr.

(E) Percentage of apoptotic cells after 72 hr.

(F) Expression of pluripotency-related genes at 72 hr.

(legend continued on next page)

the glycolytic capacity was inhibited. Moreover, when MYC inhibition by JQ-1 was combined with knockdown of *PGC1A*, the increase in mitochondrial OCR was no longer detectable (Figures S7D and S7E), thus confirming that enhanced OXPHOS in response to MYC suppression is indeed mediated by *PGC1A*. On the other hand, *MYC* overexpression induced opposite effects (Figure 7C). Strikingly, $CD133^+$ CSCs overexpressing *MYC* were no longer sensitive to mitochondrial targeting with metformin (Figure 7D), thus mimicking the metabolic phenotype of metformin-resistant CSCs, including their enhanced ability to activate the glycolytic pathway upon mitochondrial inhibition (Figure 7C). Importantly, as observed for resistant CSCs, *MYC*-overexpressing cells also showed reduced stemness features as compared to control cells (Figure 7E). These data suggest that high mitochondrial activity represents an important determinant of stemness. However, neither pluripotency genes nor sphere formation was enhanced by MYC inhibition/knockdown in differentiated cells (Figures 7E and S7F), demonstrating that the distinct metabolic features of CSCs are a prerequisite for stemness but are not sufficient to induce a CSC phenotype in non-CSCs. Even more importantly, MYC inhibition or knockdown was sufficient to prevent/reverse acquisition of resistance to metformin (Figures 7F and 7G). These results confirmed that increased *MYC* expression is indeed the mechanistic link for the altered/distinct metabolic phenotype of resistant CSC with enhanced glycolysis. Notably, MYC inhibition or knockdown also enhanced stemness of resistant CSCs, as evidenced by increased pluripotency gene expression, self-renewal capacity, and $CD133^+$ cell content (Figures 7H and 7I). These data confirm that high OXPHOS activity is mandatory for full CSC functionality.

DISCUSSION

To cope with the metabolic needs of high proliferation, cancer cells preferentially generate ATP via glycolysis, even under normoxic concentrations (Warburg effect). Similarly, highly proliferative iPS cells and somatic stem cells (e.g., hematopoietic stem cells), but interestingly also more quiescent long-term hematopoietic and neural stem cells, are also mainly glycolytic, while their respective progenies switch to OXPHOS (Shyh-Chang et al., 2013; Varum et al., 2011). The metabolic phenotype of CSCs appears to vary across tumor types. While in breast cancer and nasopharyngeal carcinoma CSCs were found to be predominantly glycolytic (Dong et al., 2013; Lin et al., 2013; Schieber and Chandel, 2013), CSCs in glioma and glioblastoma (Janiszewska et al., 2012; Vlashi et al., 2011), lung cancer (Ye et al., 2011), and leukemia (Gurumurthy et al., 2010; Lagadinou et al., 2013; Nakada et al., 2010) appear to rely on mitochondrial OXPHOS.

Here, we now show that human pancreatic CSCs, whose metabolic phenotype had not been defined to date, obtain their energy mainly through mitochondrial OXPHOS, whereas non-CSCs show the expected Warburg phenotype. Interestingly, it was recently reported that a subpopulation of murine pancreatic cancer cells, which had survived *Kras* ablation, were also mainly depending on OXPHOS (Viale et al., 2014). Similar to human CSCs described here, the authors demonstrate in *Kras*-expressing tumors the existence of a $CD133^+$ subpopulation with high mitochondrial mass and hyperpolarized mitochondria, suggesting that $CD133^+/Mito^{high}$ cells can be found in pancreatic tumors of murine and human origin. After *Kras* ablation, surviving cells were characterized by strong dependency on mitochondrial metabolism and limited metabolic plasticity, which could be attributed to the shutdown of the metabolic program driven by *Kras*. In contrast, however, we find that human CSCs derived from a large panel of PDX models, all carrying activating *KRAS* mutations identical to those found in their epigenetically defined progenies (non-CSCs), bear a distinct metabolic phenotype with limited plasticity that is controlled by *MYC*. Strikingly, CSCs from another PDX model carrying wild-type *KRAS* (PDX-354) showed a similar metabolic phenotype, further corroborating that the lack of plasticity is independent of the Kras mutational status. Moreover, *Kras*-ablated murine cells required reactivation of mutant *Kras* for proliferation and tumor relapse, suggesting that the observed OXPHOS phenotype is restricted to oncogene-ablated dormant cells, as opposed to the highly tumorigenic CSCs studied here.

Mechanistically, we found that low *MYC* expression in human CSCs allowed high *PGC1A* expression levels, which resulted in enhanced mitochondrial biogenesis, strong mitochondrial activity and antioxidant properties, and subsequently low mitochondrial ROS levels, as a prerequisite for their stemness functions. Intriguingly, sustained suppression of *MYC* was required for maintaining stemness but rendered CSCs unable to substantially activate glycolysis and thus highly susceptible to mitochondrial targeting, e.g., by metformin or menadione. *MYC* promotes a Warburg-like glycolytic phenotype, probably via dual mechanism: (1) upregulation of key glycolytic enzymes and (2) suppression of *PGC1A*. The latter is a transcriptional co-activator for nuclear receptor *PPARs*, which allows the protein to interact with multiple transcription factors, e.g., cAMP response element-binding protein (CREB) and nuclear respiratory factors (NRFs) (Fernandez-Marcos and Auwerx, 2011). While it is known that proteasomal degradation inhibits PGC-1α (Ahuja et al., 2010), we here show for the first time a direct inhibitory effect of MYC on PGC-1α at the transcriptional level, upon MYC binding to the *PGC1A* promoter.

Interestingly, while *MYC* has been linked to stemness properties in other tumors, e.g., hepatocellular carcinoma, breast, and lung cancer (Akita et al., 2014; Zhao et al., 2015), we found in PDAC that *MYC* was associated with a more differentiated phenotype and *MYC* overexpression actually reduced stemness in CSCs (Figure 7). Notably, while suppression of *MYC* was essential for maintaining CSC phenotypes, the mere inhibition of *MYC* in non-CSCs did not equip them with stemness features.

(G) Sphere formation after 7 days. Cells/tumors were pretreated for 5 days in vitro or treated for 15 days in vivo.
(H) Respective data for surface expression of CD133.
(I) In vivo tumorigenicity assay. 10^3 or 10^4 cells from PDX-215 and 354 were pretreated for 7 days with the indicated inhibitors and then injected into mice. Top left: table summarizing the number of tumors obtained after 15 weeks. Bottom: representative images of tumors obtained for PDX-215cells. Top right: kinetics of tumor take upon injection of 10^3 PDX-215 cells.
Data are presented as mean ± SEM. *$p < 0.05$, **$p < 0.01$, ***$p < 0.001$. See also Figure S4.

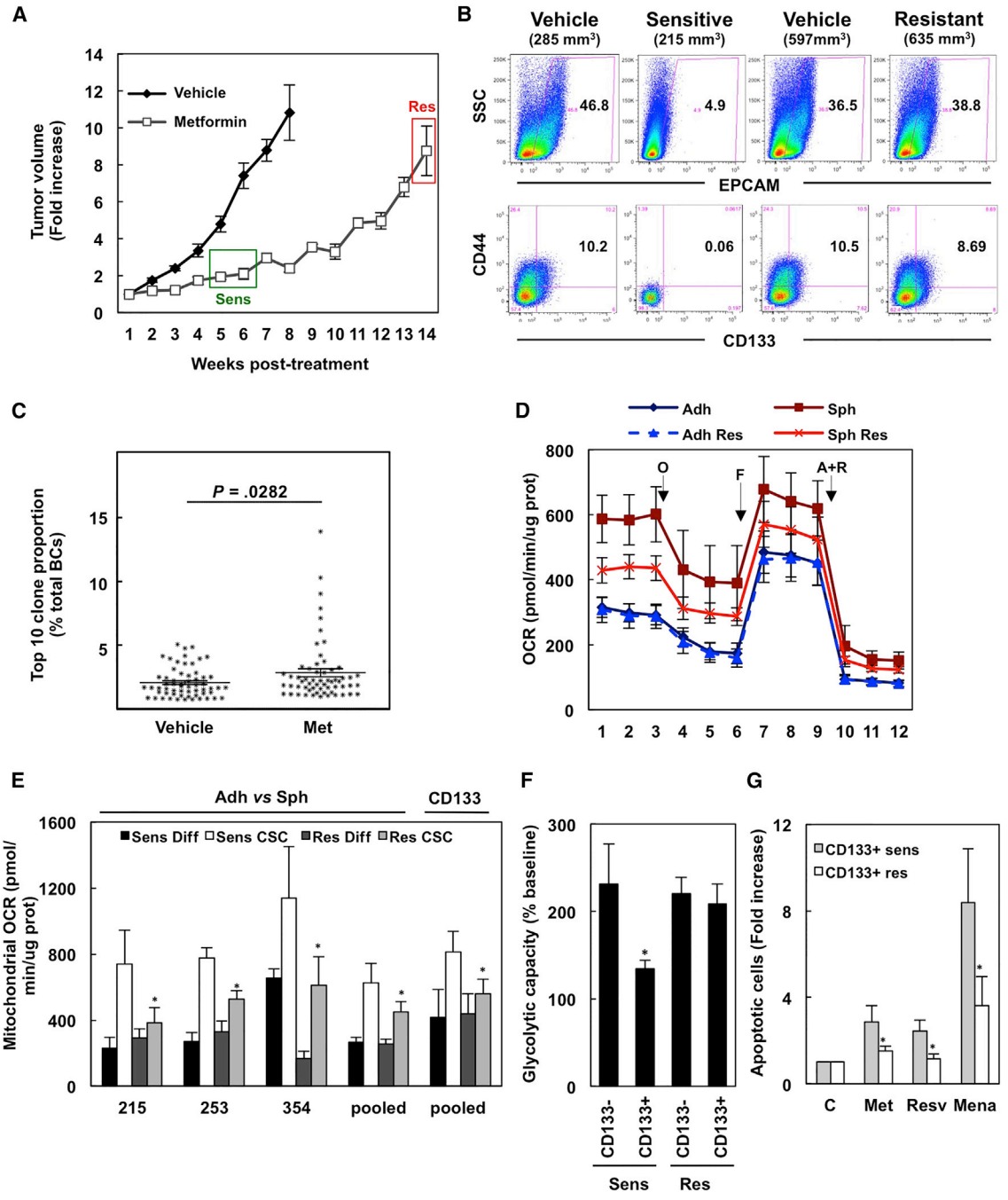

Figure 5. Metformin-Resistant CSCs Display an Intermediate Metabolic Phenotype

PDX-A6L, 185, and 286 tissue was implanted, and once tumors had reached an average volume of 100 mm^3, mice were randomized for 150 mg/Kg/day metformin or vehicle.

(A) Tumor growth curves. Squares indicate when sensitive and resistant tumors, respectively, were harvested.

(B) EPCAM (top panel) and CD44/CD133 (bottom panel) staining was assessed by flow cytometry. Size-matched tumors were treated with vehicle or metformin.

(C) Percentage of tumor composed by the most abundant individual barcodes, following 6 weeks of treatment.

(D) OCR measurements. O, oligomycin; F, FCCP; A+R, antimycin + rotenone.

(E) Mitochondrial OCR.

(F) Glycolytic capacity after Glc+oligomycin injection, comparing CD133– and CD133+ cells obtained from either sensitive or resistant cultures.

(G) Apoptosis induction in $CD133^+$ cells derived from sensitive and resistant cultures upon 72 hr of treatment.

Data in (A) and (C)–(G) are presented as mean ± SEM. *p < 0.05, **p < 0.01, ***p < 0.001. See also Figure S5.

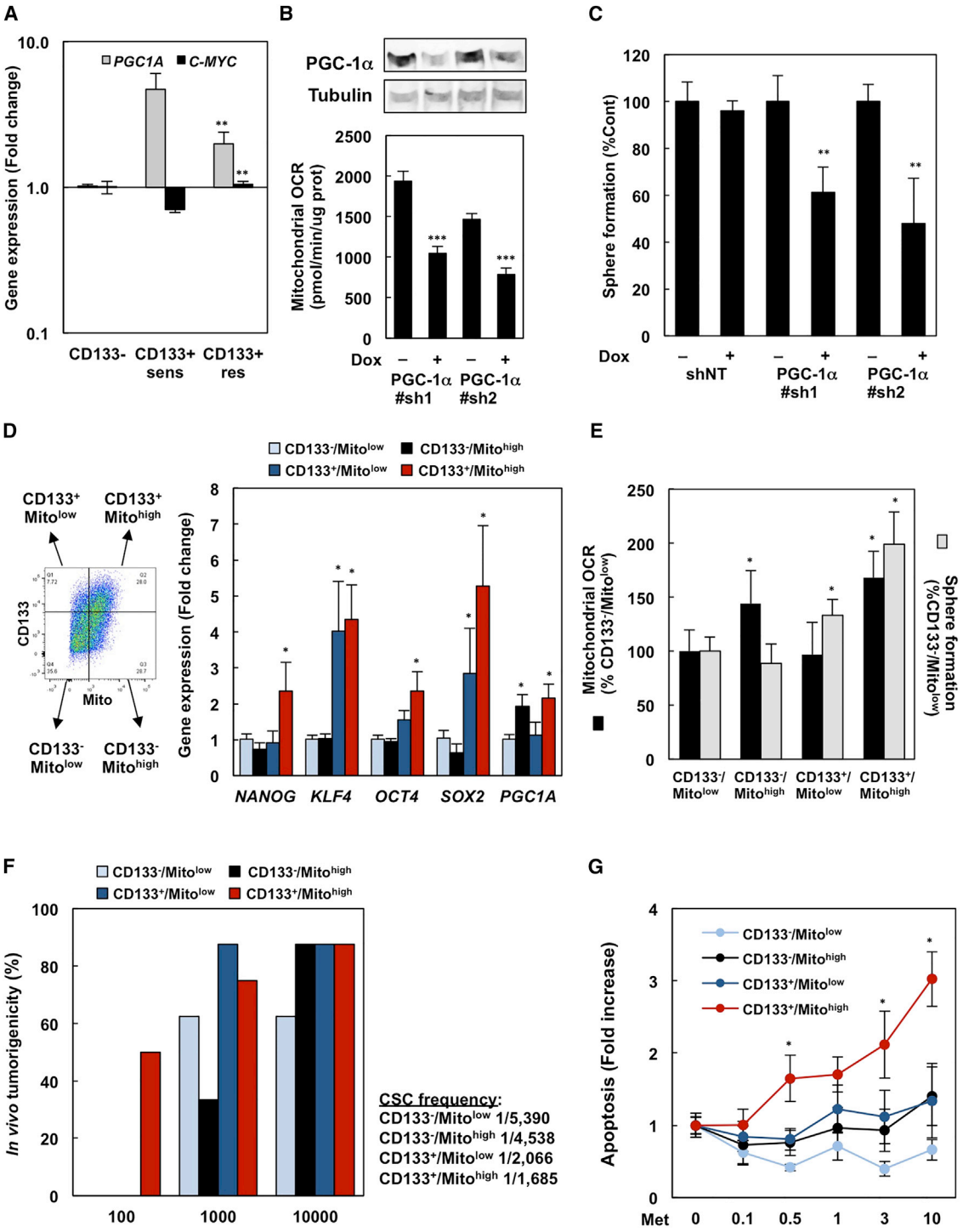

Figure 6. MYC/PGC-1α Ratio Determines the Metabolic Phenotype of CSC

(A) *PGC1A* and *MYC* expression as determined by real-time PCR in treatment-naive CD133$^+$ versus CD133$^-$ cells derived from either sensitive or resistant cultures. Data are represented at logarithmic scale, relative to CD133– cells. Pooled data from PDX-215, 253, and 354.

(B) PDX-215 cells were transduced with two different inducible shRNA lentiviral constructs against PGC-1α and then cultured in the presence or absence of 2 ng/ml doxycycline. PGC-1α levels as assessed by western blot (top panel) and mitochondrial OCR (bottom panel).

(C) Sphere formation upon knockdown of PGC-1α.

(D) Left, representative CD133/mitochondrial mass staining. Right, expression of pluripotency-related genes and *PGC1A* in the sorted populations.

(E) Mitochondrial OCR (black bars) and sphere formation capacity (gray bars).

(legend continued on next page)

In addition, building on prior evidence that PGC-1α is crucial for the anti-oxidative capacity and mitochondrial metabolism in cancer (Haq et al., 2013; LeBleu et al., 2014; Vazquez et al., 2013), we now demonstrate that PGC-1α also maintains CSC self-renewal capacity, probably by controlling intracellular ROS levels. Importantly, metformin-resistant CSCs display decreased PGC-1α levels and thus enhanced intracellular ROS levels, which negatively impacted their self-renewal capacity but still allowed them to promote disease relapse in the presence of metformin. Together, these data indicate that the distinct metabolic features of CSCs are a prerequisite for CSC functions in PDAC, but other cell-specific signals, e.g., Nodal/Activin, are required for the CSC phenotype (Lonardo et al., 2011).

Our data also suggest that the metabolic phenotype of CSCs is heterogeneous. While the majority of CSCs was depending on OXPHOS with very limited metabolic plasticity, a subset of CSCs that was small in treatment naive tumors but strongly expanded in metformin-resistant tumors, was characterized by an intermediate and more adaptable metabolic phenotype. These cells were identified as $CD133^{+}/Mito^{low}$ cells and showed reduced mitochondrial mass and stemness but also enhanced metabolic plasticity and inherent resistance to metformin (Figures 6D–6G). The diminished clonal heterogeneity found in metformin-resistant tumors and their global intermediate phenotype, reminiscent of above $CD133^{+}/Mito^{low}$ cells (Figure 5C), strongly suggests that pre-existing metabolic heterogeneity in pancreatic CSCs is the main driver of relapse under metformin treatment.

Indeed, while epidemiological and preclinical evidence was strongly supporting the use of metformin as a new treatment option for pancreatic cancer, first clinical trials have been disappointing (Carvalho et al., 2014; Kordes et al., 2015; Wilmink et al., 2014). Dosage has been a main concern for this apparent lack of translatability. In the clinic, metformin is administered at anti-diabetic doses (500–1,000 mg/day), which corresponds to the 250 mg/kg/day in mice, and regularly results in plasma concentrations in the micromolar range. In vitro inhibition of cancer cell proliferation, however, has been reported for millimolar concentrations (Lonardo et al., 2013; Rizos and Elisaf, 2013). Notably, glucose levels are an important determinant of metformin response. As opposed to the usual hyperglycemic cell culture conditions (e.g., 17.5 mM in DMEM/F-12), the required metformin dose for targeting CSCs in normal or low Glc conditions (5 mM and 1 mM, respectively) is substantially lower (100 μM, Figure 3B) and in fact does correspond to achievable plasma concentrations in vivo. Moreover, at least in mice using the above dosing scheme, substantial tumor inhibition including a significant depletion of the CSC content has been achieved, even though these effects were not lasting (Lonardo et al., 2013; Oliveras-Ferraros et al., 2014). Thus, the outgrowth of drug-resistant CSC clones during metformin treatment could at least in part explain the limited response in patients.

Intriguingly, in the present study, no resistance was observed for another mitochondria-targeting agent, i.e., menadione. As opposed to metformin, the compound is undergoing futile redox cycles on the respiratory chain subsequently inducing ROS (Petronilli et al., 1994). Therefore, menadione is likely to affect CSC functionality by dual mechanism, oxidizing several mitochondrial proteins as well as inducing mitochondrial ROS that alter the intricate redox equilibrium critical for maintaining both survival and self-renewal of CSCs (Diehn et al., 2009). This may explain the lack of resistance to menadione and thus may represent an interesting new opportunity for mitochondrial targeting in PDAC. Alternatively, combining metformin with MYC inhibition, e.g., using the BRD4 inhibitor JQ-1, prevented or reversed, respectively, resistance to metformin by enforcing their dependence on OXPHOS, suggesting a new multimodal approach for targeting the distinct metabolic features of pancreatic CSCs.

EXPERIMENTAL PROCEDURES

Primary Human PDAC Cells

For primary cultures, PDX-derived tumor tissue fragments were minced, enzymatically digested with collagenase (Stem Cell Technologies) for 90 min at 37°C (Mueller et al., 2009), and after centrifugation for 5 min at 1,200 rpm the pellets were resuspended and cultured in RPMI, 10% FBS, and 50 units/ml penicillin/streptomycin.

Cancer Stem Cell-Enriching Culture

PDAC spheres were generated and expanded in DMEM-F12 (Invitrogen) supplemented with B-27 (GIBCO) and bFGF (PeproTech EC). 10^3 cells/ml were seeded in ultra-low attachment plates (Corning) as described previously (Gallmeier et al., 2011). For serial passaging, spheres were harvested at day 7 using a 40 μm cell strainer, dissociated to single cells with trypsin, and then re-grown in the same conditions for 7 days. Number of spheres >40 μm were determined using a CASY Cell Counter (Roche).

Flow Cytometry and Cell Sorting

Primary pancreatic cells (adherent monolayers or dissociated cells from sphere cultures) were resuspended in Sorting buffer (1× PBS; 3% FBS [v/v]; 3 μM EDTA [v/v]) before analysis or sorting with a FACS Canto II or FACS Influx instrument, respectively (BD). To identify pancreatic CSCs, the following antibodies were used: anti-CD133/1-APC or PE; (Miltenyi), anti-CXCR4-APC, SSEA-1-APC, EPCAM-FITC, CD44-PE (all from eBiosciences), or appropriate isotype-matched control antibodies. DAPI was used for exclusion of dead cells (eBiosciences). All samples were analyzed by flow cytometry using a FACS Canto II (BD), and data were analyzed with FlowJo 9.2 software (Tree Star).

XF Extracellular Flux Analyzer Experiments

Single-cell suspensions from trypsinized secondary spheres/adherent cultures or cells sorted for CD133 were plated in XF96 Cell Culture Microplates (Seahorse Bioscience) previously coated with Cell-Tak (BD Biosciences) at a cellular density of 30,000 cells/well. For OCR determination, cells were incubated in base assay medium (D5030, Sigma) supplemented with 2 mM glutamine, 10 mM glucose, and 1 mM pyruvate for 1 hr, prior to the measurements using the XF Cell Mito Stress Kit (Seahorse Bioscience). Concentrations of oligomycin and FCCP were adjusted for each primary cell type. For glycolytic metabolism measurements, cells were incubated in basal media prior to injections using the Glycolytic Test kit (Seahorse Bioscience). For evaluation of the response to metformin, 3 mM metformin was injected in ports A–C, and percentage of complex I inhibition was calculated as the percentage of OCR inhibited upon metformin injection with respect to the inhibition obtained with rotenone, used as 100%. Alternatively, sequential injection of metformin, FCCP, and antimycin + rotenone versus rotenone, FCCP, and antimycin were

(F) Left, percentage of tumors obtained after injection of indicated numbers of cells. Right, CSC frequency, calculated from tumorigenicity data using ELDA software.

(G) Apoptosis upon 72 hr treatment with metformin.

Data are presented as mean ± SEM. *p < 0.05, **p < 0.01, ***p < 0.001.

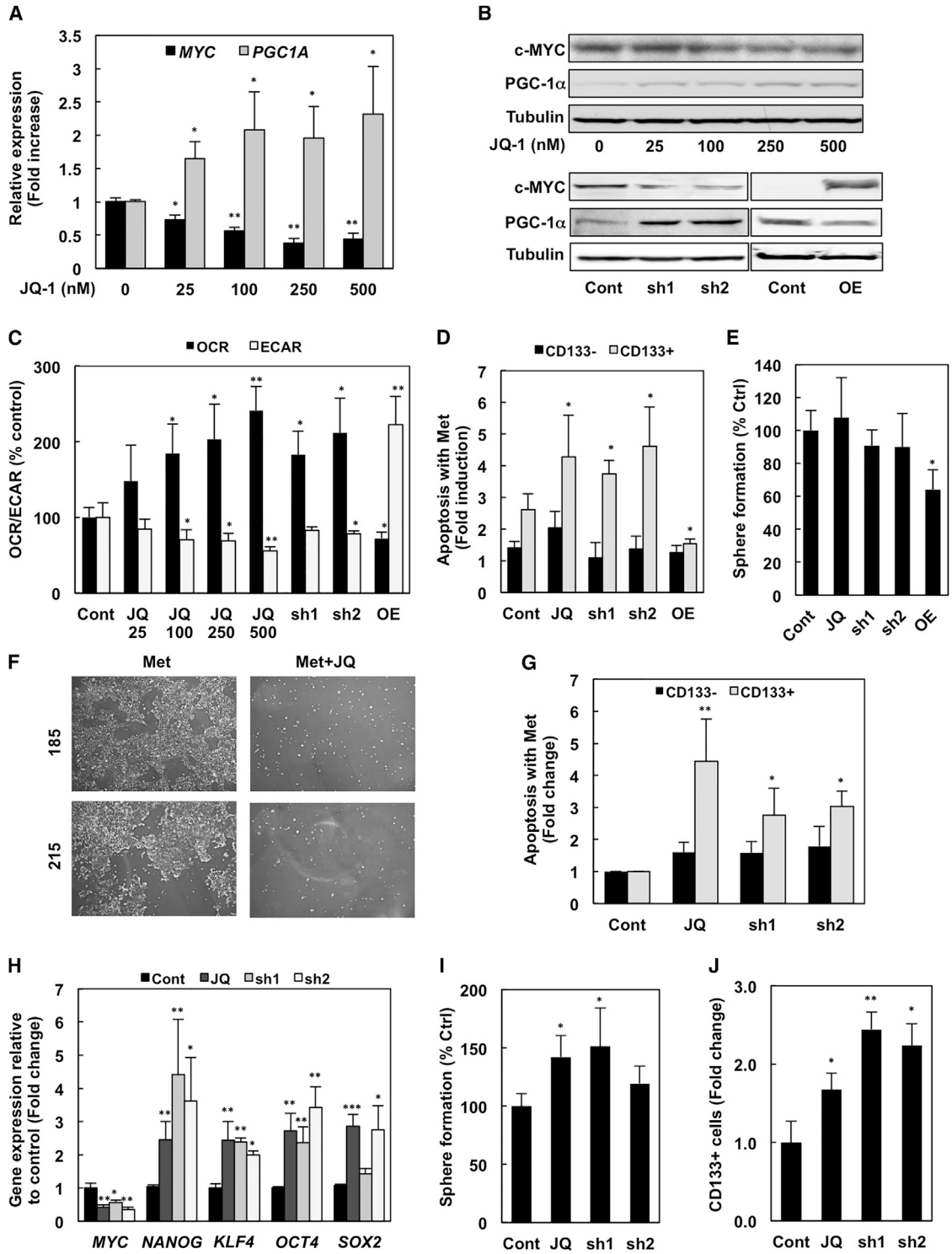

Figure 7. MYC Inhibition Increases Mitochondrial Respiration, Restoring Response to Metformin and Full Stemness in Metformin-Resistant Cells

(A–E) Parental PDX-215 cells or 215 expressing either two different inducible lentiviral MYC shRNA constructs (sh1, sh2) or a MYC overexpression construct (OE) were used.

(A) *PGC1A* and *MYC* mRNA expression levels in cells treated for 72 hr with increasing concentrations of the MYC inhibitor JQ-1.

(B) PGC-1α and MYC protein expression levels. Tubulin was used as loading control.

(C) Mitochondrial OCR and glycolytic capacity.

(D) Apoptosis as assessed by Annexin/DAPI staining, upon 72 hr of metformin treatment.

(legend continued on next page)

carried out. Experiments were run in a XF96 analyzer (Seahorse Bioscience), and raw data were normalized to protein content.

In Vivo Tumorigenicity Assay

Pretreated/sorted cells were trypsinized, resuspended in 50 μl of Matrigel, and then subcutaneously injected into female 6- to 8-week-old NU-*Foxn1*^{nu} nude mice (Harlan Laboratories). Tumor growth was monitored weekly for up to 4 months. Procedures were conducted in accordance with the institutional and national regulations (Ethics Committee of the Instituto de Salud Carlos III, Madrid, Spain; Protocol PA 34_2012 and Animals in Science Regulation Unit, Home Office Science, London, UK; Project License PPL70/8129).

In Vivo Treatments

NU-Foxn1nu nude mice (6–8 weeks of age) were purchased from Charles Rivers or Harlan Laboratories. Tumor pieces were subcutaneously implanted, and when tumors reached a volume of 100 mm^3, mice were randomized into treatment groups: metformin (drinking water, 150 mg/kg), resveratrol (subcutaneous, 25 mg/kg), menadione (i.p., 20 mg/kg), and rotenone (subcutaneous, 0.5 mg/kg). For CSC evaluation, mice were sacrificed after 15 days of treatment, tumors digested, and assessed for CD44+CD133+ CSC content and sphere formation capacity. Mice were housed according to institutional guidelines, and procedures were conducted in accordance with the institutional and national regulations (Ethics Committee of the Instituto de Salud Carlos III, Madrid, Spain; Protocol PA 34_2012 and Animals in Science Regulation Unit, Home Office Science, London, UK; Project License PPL70/8129).

RNA-Seq Library Construction and Analysis Method

Total RNA was isolated by the guanidine thiocyanate method using standard protocols. PolyA+ RNA fraction was processed as in Illumina's "TruSeq RNA Sample Preparation v2 Protocol" (Part # 15026494 Rev. C). The resulting purified cDNA library was applied to an Illumina flow cell for cluster generation (TruSeq cluster generation kit v5) and sequenced on the Genome Analyzer IIx with SBS TruSeq v5 reagents by following manufacturer's protocols. Transcript assembly and estimation of their abundances were calculated with Cufflinks 1.3.0 (Trapnell et al., 2012), using the human genome annotation dataset Homo_sapiens.GRCh37.65 from Ensembl (Flicek et al., 2014). Differential expression for genes across the different conditions was calculated with Cuffdiff (Trapnell et al., 2012). Principal component analysis (PCA) figures showing how samples clustered was obtained with R (http://www.r-project.org/). Heatmaps showing gene expression levels (in FPKM, fragments per kilobase of transcript per million mapped fragments) through the different samples were drawn with GENE-E (http://www.broadinstitute.org/cancer/software/GENE-E/) for a subset of selected genes. Data deposited in ArrayExpress: E-MTAB-3808. More details are available in the Supplemental Information.

Statistical Analyses

Results for continuous variables are presented as means ± SEM unless stated otherwise. Treatment groups were compared with the independent samples t test. Pair-wise multiple comparisons were performed with the one-way ANOVA (two-sided) with Bonferroni adjustment. p values < 0.05 were considered statistically significant. All analyses were performed using SPSS 22.0 (SPSS). Full description of Experimental Procedures is available in the Supplemental Information.

ACCESSION NUMBERS

The Array Express accession number for the RNA-seq experiment reported in this paper is E-MTAB-3808.

SUPPLEMENTAL INFORMATION

Supplemental Information includes Supplemental Experimental Procedures and seven figures and can be found with this article online at http://dx.doi.org/10.1016/j.cmet.2015.08.015.

AUTHOR CONTRIBUTIONS

P.S. acquired, analyzed, and interpreted data as well as developed the study concept and wrote the manuscript; E.B. and A.T. acquired and analyzed in vitro data; P.J. performed in vivo experiments; M.S. extracted and analyzed barcode data; D.B. and K.S. acquired and analyzed GC-MS data; R.C.O. acquired and analyzed NMR data; O.G. analyzed RNA-seq data; T.B. performed the ChIP and *PGC1A* promoter experiments; C.R.V. designed and produced the lentiviral constructs; M.Y. interpreted GC-MS data; B.S. obtained and interpreted RNA sequencing data and helped with the development of the study concept; and C.H. developed the study concept, obtained funding, interpreted the data, and wrote the manuscript.

ACKNOWLEDGMENTS

The research was supported by the ERC Advanced Investigator Grant (Pa-CSC 233460), European Community's Seventh Framework Programme (FP7/2007-2013) under grant agreement number 256974 (EPC-TM-NET) and number 602783 (CAM-PaC), the Subdirección General de Evaluación y Fomento de la Investigación, Fondo de Investigación Sanitaria (PS09/02129 & PI12/02643), and the Programa Nacional de Internacionalización de la I+D, Subprogramma: FCCI 2009 (PLE2009-0105; both Ministerio de Economía y Competitividad [es], Spain).

Received: December 20, 2014
Revised: June 25, 2015
Accepted: August 11, 2015
Published: September 10, 2015

REFERENCES

Ahuja, P., Zhao, P., Angelis, E., Ruan, H., Korge, P., Olson, A., Wang, Y., Jin, E.S., Jeffrey, F.M., Portman, M., and Maclellan, W.R. (2010). Myc controls transcriptional regulation of cardiac metabolism and mitochondrial biogenesis in response to pathological stress in mice. J. Clin. Invest. *120*, 1494–1505.

Akita, H., Marquardt, J.U., Durkin, M.E., Kitade, M., Seo, D., Conner, E.A., Andersen, J.B., Factor, V.M., and Thorgeirsson, S.S. (2014). MYC activates stem-like cell potential in hepatocarcinoma by a p53-dependent mechanism. Cancer Res. *74*, 5903–5913.

Batandier, C., Guigas, B., Detaille, D., El-Mir, M.Y., Fontaine, E., Rigoulet, M., and Leverve, X.M. (2006). The ROS production induced by a reverse-electron flux at respiratory-chain complex 1 is hampered by metformin. J. Bioenerg. Biomembr. *38*, 33–42.

Carvalho, A., Flesch, T.E., Alex, A.K., Nebuloni, D.R., Carneiro, A.Q., Capareli, F.C., and Riechelman, R.P. (2014). Phase II trial of metformin and paclitaxel for patients with gemcitabine-refractory advanced adenocarcinoma of the pancreas. Journal of clinical oncology: official journal of the American Society of Clinical Oncology *32*, e15196.

Diehn, M., Cho, R.W., Lobo, N.A., Kalisky, T., Dorie, M.J., Kulp, A.N., Qian, D., Lam, J.S., Ailles, L.E., Wong, M., et al. (2009). Association of reactive

(E) Sphere formation assay.
(F) PDX-185 and 215 cells were treated for 21 days with metformin alone or in combination with JQ-1, and subsequently cultured for 21 more days in the absence of treatment to evaluate the emergence of resistant clones.
(G–J) Parental metformin-resistant cells or cells expressing different inducible lentiviral MYC shRNA constructs were used.
(G) Apoptosis induction in metformin-resistant cells upon 72 hr treatment with metformin in the absence or presence of JQ-1 or doxycycline for shRNA induction.
(H) Expression of mRNA for pluripotency genes.
(I) Sphere formation assay.
(J) Content of CD133$^+$ cells. Data are presented as mean ± SEM. *p < 0.05, **p < 0.01, ***p < 0.001. See also Figure S7.

oxygen species levels and radioresistance in cancer stem cells. Nature *458*, 780–783.

Dong, C., Yuan, T., Wu, Y., Wang, Y., Fan, T.W., Miriyala, S., Lin, Y., Yao, J., Shi, J., Kang, T., et al. (2013). Loss of FBP1 by Snail-mediated repression provides metabolic advantages in basal-like breast cancer. Cancer Cell *23*, 316–331.

Fernandez-Marcos, P.J., and Auwerx, J. (2011). Regulation of PGC-1α, a nodal regulator of mitochondrial biogenesis. Am. J. Clin. Nutr. *93*, 884S–90.

Flicek, P., Amode, M.R., Barrell, D., Beal, K., Billis, K., Brent, S., Carvalho-Silva, D., Clapham, P., Coates, G., Fitzgerald, S., et al. (2014). Ensembl 2014. Nucleic Acids Res. *42*, D749–D755.

Gallmeier, E., Hermann, P.C., Mueller, M.T., Machado, J.G., Ziesch, A., De Toni, E.N., Palagyi, A., Eisen, C., Ellwart, J.W., Rivera, J., et al. (2011). Inhibition of ataxia telangiectasia- and Rad3-related function abrogates the in vitro and in vivo tumorigenicity of human colon cancer cells through depletion of the CD133(+) tumor-initiating cell fraction. Stem Cells *29*, 418–429.

Gurumurthy, S., Xie, S.Z., Alagesan, B., Kim, J., Yusuf, R.Z., Saez, B., Tzatsos, A., Ozsolak, F., Milos, P., Ferrari, F., et al. (2010). The Lkb1 metabolic sensor maintains haematopoietic stem cell survival. Nature *468*, 659–663.

Haq, R., Shoag, J., Andreu-Perez, P., Yokoyama, S., Edelman, H., Rowe, G.C., Frederick, D.T., Hurley, A.D., Nellore, A., Kung, A.L., et al. (2013). Oncogenic BRAF regulates oxidative metabolism via PGC1α and MITF. Cancer Cell *23*, 302–315.

Hermann, P.C., Huber, S.L., Herrler, T., Aicher, A., Ellwart, J.W., Guba, M., Bruns, C.J., and Heeschen, C. (2007). Distinct populations of cancer stem cells determine tumor growth and metastatic activity in human pancreatic cancer. Cell Stem Cell *1*, 313–323.

Hidalgo, M. (2010). Pancreatic cancer. N. Engl. J. Med. *362*, 1605–1617.

Jackstadt, R., and Hermeking, H. (2015). MicroRNAs as regulators and mediators of c-MYC function. Biochim. Biophys. Acta *1849*, 544–553.

Janiszewska, M., Suvà, M.L., Riggi, N., Houtkooper, R.H., Auwerx, J., Clément-Schatlo, V., Radovanovic, I., Rheinbay, E., Provero, P., and Stamenkovic, I. (2012). Imp2 controls oxidative phosphorylation and is crucial for preserving glioblastoma cancer stem cells. Genes Dev. *26*, 1926–1944.

Jimeno, A., Feldmann, G., Suárez-Gauthier, A., Rasheed, Z., Solomon, A., Zou, G.M., Rubio-Viqueira, B., García-García, E., López-Ríos, F., Matsui, W., et al. (2009). A direct pancreatic cancer xenograft model as a platform for cancer stem cell therapeutic development. Mol. Cancer Ther. *8*, 310–314.

Kordes, S., Pollak, M.N., Zwinderman, A.H., Mathôt, R.A., Weterman, M.J., Beeker, A., Punt, C.J., Richel, D.J., and Wilmink, J.W. (2015). Metformin in patients with advanced pancreatic cancer: a double-blind, randomised, placebo-controlled phase 2 trial. Lancet Oncol. *16*, 839–847.

Lagadinou, E.D., Sach, A., Callahan, K., Rossi, R.M., Neering, S.J., Minhajuddin, M., Ashton, J.M., Pei, S., Grose, V., O'Dwyer, K.M., et al. (2013). BCL-2 inhibition targets oxidative phosphorylation and selectively eradicates quiescent human leukemia stem cells. Cell Stem Cell *12*, 329–341.

LeBleu, V.S., O'Connell, J.T., Gonzalez Herrera, K.N., Wikman, H., Pantel, K., Haigis, M.C., de Carvalho, F.M., Damascena, A., Domingos Chinen, L.T., Rocha, R.M., et al. (2014). PGC-1α mediates mitochondrial biogenesis and oxidative phosphorylation in cancer cells to promote metastasis. Nat. Cell Biol. *16*, 992–1003, 1–15.

Li, C., Heidt, D.G., Dalerba, P., Burant, C.F., Zhang, L., Adsay, V., Wicha, M., Clarke, M.F., and Simeone, D.M. (2007). Identification of pancreatic cancer stem cells. Cancer Res. *67*, 1030–1037.

Lin, C.H., Hung, P.H., and Chen, Y.J. (2013). CD44 Is Associated with the Aggressive Phenotype of Nasopharyngeal Carcinoma through Redox Regulation. Int. J. Mol. Sci. *14*, 13266–13281.

Lonardo, E., Hermann, P.C., Mueller, M.T., Huber, S., Balic, A., Miranda-Lorenzo, I., Zagorac, S., Alcala, S., Rodriguez-Arabaolaza, I., Ramirez, J.C., et al. (2011). Nodal/Activin signaling drives self-renewal and tumorigenicity of pancreatic cancer stem cells and provides a target for combined drug therapy. Cell Stem Cell *9*, 433–446.

Lonardo, E., Cioffi, M., Sancho, P., Sanchez-Ripoll, Y., Trabulo, S.M., Dorado, J., Balic, A., Hidalgo, M., and Heeschen, C. (2013). Metformin targets the metabolic achilles heel of human pancreatic cancer stem cells. PLoS ONE *8*, e76518.

Miranda-Lorenzo, I., Dorado, J., Lonardo, E., Alcala, S., Serrano, A.G., Clausell-Tormos, J., Cioffi, M., Megias, D., Zagorac, S., Balic, A., et al. (2014). Intracellular autofluorescence: a biomarker for epithelial cancer stem cells. Nat. Methods *11*, 1161–1169.

Mueller, M.T., Hermann, P.C., Witthauer, J., Rubio-Viqueira, B., Leicht, S.F., Huber, S., Ellwart, J.W., Mustafa, M., Bartenstein, P., D'Haese, J.G., et al. (2009). Combined targeted treatment to eliminate tumorigenic cancer stem cells in human pancreatic cancer. Gastroenterology *137*, 1102–1113.

Nakada, D., Saunders, T.L., and Morrison, S.J. (2010). Lkb1 regulates cell cycle and energy metabolism in haematopoietic stem cells. Nature *468*, 653–658.

Nalls, D., Tang, S.N., Rodova, M., Srivastava, R.K., and Shankar, S. (2011). Targeting epigenetic regulation of miR-34a for treatment of pancreatic cancer by inhibition of pancreatic cancer stem cells. PLoS ONE *6*, e24099.

Oliveras-Ferraros, C., Vazquez-Martin, A., Cuyàs, E., Corominas-Faja, B., Rodríguez-Gallego, E., Fernández-Arroyo, S., Martin-Castillo, B., Joven, J., and Menendez, J.A. (2014). Acquired resistance to metformin in breast cancer cells triggers transcriptome reprogramming toward a degradome-related metastatic stem-like profile. Cell Cycle *13*, 1132–1144.

Petronilli, V., Costantini, P., Scorrano, L., Colonna, R., Passamonti, S., and Bernardi, P. (1994). The voltage sensor of the mitochondrial permeability transition pore is tuned by the oxidation-reduction state of vicinal thiols. Increase of the gating potential by oxidants and its reversal by reducing agents. J. Biol. Chem. *269*, 16638–16642.

Rahib, L., Smith, B.D., Aizenberg, R., Rosenzweig, A.B., Fleshman, J.M., and Matrisian, L.M. (2014). Projecting cancer incidence and deaths to 2030: the unexpected burden of thyroid, liver, and pancreas cancers in the United States. Cancer Res. *74*, 2913–2921.

Rizos, C.V., and Elisaf, M.S. (2013). Metformin and cancer. Eur. J. Pharmacol. *705*, 96–108.

Schieber, M.S., and Chandel, N.S. (2013). ROS links glucose metabolism to breast cancer stem cell and EMT phenotype. Cancer Cell *23*, 265–267.

Shyh-Chang, N., Daley, G.Q., and Cantley, L.C. (2013). Stem cell metabolism in tissue development and aging. Development *140*, 2535–2547.

Siegel, R., Naishadham, D., and Jemal, A. (2012). Cancer statistics, 2012. CA Cancer J. Clin. *62*, 10–29.

Trapnell, C., Roberts, A., Goff, L., Pertea, G., Kim, D., Kelley, D.R., Pimentel, H., Salzberg, S.L., Rinn, J.L., and Pachter, L. (2012). Differential gene and transcript expression analysis of RNA-seq experiments with TopHat and Cufflinks. Nat. Protoc. *7*, 562–578.

Varum, S., Rodrigues, A.S., Moura, M.B., Momcilovic, O., Easley, C.A., 4th, Ramalho-Santos, J., Van Houten, B., and Schatten, G. (2011). Energy metabolism in human pluripotent stem cells and their differentiated counterparts. PLoS ONE *6*, e20914.

Vazquez, F., Lim, J.H., Chim, H., Bhalla, K., Girnun, G., Pierce, K., Clish, C.B., Granter, S.R., Widlund, H.R., Spiegelman, B.M., and Puigserver, P. (2013). PGC1α expression defines a subset of human melanoma tumors with increased mitochondrial capacity and resistance to oxidative stress. Cancer Cell *23*, 287–301.

Viale, A., Pettazzoni, P., Lyssiotis, C.A., Ying, H., Sanchez, N., Marchesini, M., Carugo, A., Green, T., Seth, S., Giuliani, V., et al. (2014). Oncogene ablation-resistant pancreatic cancer cells depend on mitochondrial function. Nature *514*, 628–632.

Vlashi, E., Lagadec, C., Vergnes, L., Matsutani, T., Masui, K., Poulou, M., Popescu, R., Della Donna, L., Evers, P., Dekmezian, C., et al. (2011). Metabolic state of glioma stem cells and nontumorigenic cells. Proc. Natl. Acad. Sci. USA *108*, 16062–16067.

Wilmink, J., Kordes, S., Zwinderman, K., Mathot, R., Cornelis, J.A., and Richel, D. (2014). A phase II randomized, placebo controlled study to evaluate the efficacy of the combination of gemcitabine, erlotinib, and metformin in

patients with locally advanced or metastatic pancreatic cancer. J. Clin. Oncol. *32*, 4021.

Wu, M., Neilson, A., Swift, A.L., Moran, R., Tamagnine, J., Parslow, D., Armistead, S., Lemire, K., Orrell, J., Teich, J., et al. (2007). Multiparameter metabolic analysis reveals a close link between attenuated mitochondrial bioenergetic function and enhanced glycolysis dependency in human tumor cells. Am. J. Physiol. Cell Physiol. *292*, C125–C136.

Ye, X.Q., Li, Q., Wang, G.H., Sun, F.F., Huang, G.J., Bian, X.W., Yu, S.C., and Qian, G.S. (2011). Mitochondrial and energy metabolism-related properties as novel indicators of lung cancer stem cells. Int. J. Cancer *129*, 820–831.

Zhao, D., Pan, C., Sun, J., Gilbert, C., Drews-Elger, K., Azzam, D.J., Picon-Ruiz, M., Kim, M., Ullmer, W., El-Ashry, D., et al. (2015). VEGF drives cancer-initiating stem cells through VEGFR-2/Stat3 signaling to upregulate Myc and Sox2. Oncogene *34*, 3107–3119.